Plant Cell, Tissue and Organ Culture (PCTOC) (2024) 156:65
https://doi.org/10.1007/s11240-023-02624-1

ORIGINAL ARTICLE

Isolation, heterologous expression, and functional determination of an iron regulated transporter (IRT) gene involved in Fe^{2+} transport and tolerance to Fe^{2+} deficiency in *Vitis vinifera*

Zhizhong Song[1,2,3] · Xue Wang[1] · Mengyuan Li[1] · Youzheng Ning[2] · Shengpeng Shi[2,3] · Guangrong Yang[4] · Hongxia Zhang[1] · Meiling Tang[1,5] · Bin Peng[1,4]

Received: 27 May 2023 / Accepted: 15 November 2023 / Published online: 23 January 2024

Abstract

In plants, iron (Fe) regulated transporters (IRT) play important roles in uptake and transport of Fe that contributes to plant growth and development. However, biological functions of IRT transporters in fruit trees are still unknown. This study isolated 10 *VvIRT* genes from 'Marselan' grape, with varying expression levels across different tissues/organs, particularly enhanced under Fe depletion, especially in roots. Notably, *VvIRT7* is the most abundantly expressed *IRT* gene in grape, beneficially restoring the Fe^{2+} uptake defect of yeast mutant DEY1453. Furthermore, *VvIRT7* showed dominant expression in the roots of *irt1*/35S::*IRT7* complementation lines. Overexpressing of *VvIRT7* rescued the retarded growth of *irt1* knockout mutant, by increasing the fresh weight, dry weight, total root length, total root surface, lateral root numbers, total leaf chlorophyll, ACO activity, NiR activity, SDH activity, and tissue Fe concentration. This study provides insights for understanding molecular mechanisms of Fe uptake and transport in grape.

Key message

A grape iron regulated transporter gene involved in Fe^{2+} transport and resistance to Fe^{2+} deficiency was isolated, heterologously expressed, and functionally characterized.

Keywords Grape · Fe uptake and transport · Fe regulated transporter · Heterologous expression · Tissue Fe staining

Introduction

Iron (Fe) is one of the abundant microelements in plant cells. It participates in many metabolic pathways and life processes, such as photosynthesis, respiration, hormone synthesis, energy metabolism, and DNA repair (Barton and Abadia 2006; Lill 2009; Couturier et al. 2013; Song et al. 2022). Notably, Fe deficiency in soils seriously decreases crop yield and reduces quality (Tagliavini et al. 2000; Tagliavini and Rombolà 2001; Kobayashi and Nishizawa 2012).

Higher plants implement two kinds of root Fe absorption strategies to adapt to Fe deficiency stress (Kobayashi and Nishizawa 2012; Zelazny and Vert 2015; Fourcroy et al. 2016; Zhang et al. 2019, 2021; Mondal et al. 2022). Strategy I is common in dicotyledons and non-gramineous monocotyledons. In this strategy, H^+ is secreted into the rhizosphere through H^+-ATPase located on the surface of root cell membrane. This action lowers the pH value of surrounding

Communicated by S.J. Ochatt.

✉ Zhizhong Song
3614@ldu.edu.cn

✉ Bin Peng
bingo1937@foxmail.com

1 The Engineering Research Institute of Agriculture and Forestry, Ludong University, No. 186 Hongqizhong Road, Yantai 264025, China

2 Department of Plant Science, University of Cambridge, Downing Street, Cambridge CB2 3EA, UK

3 Wolfson College, University of Cambridge, Barton Road, Cambridge CB3 9BB, UK

4 Jiangsu Vocational College of Agriculture and Forestry, Wenchangdong Road, Zhenjiang 212499, China

5 Yantai Academy of Agricultural Sciences, No. 26 West Gangcheng Street, Yantai 265500, China

soil, promotes the dissolution of Fe^{3+}, and reduces Fe^{3+} to Fe^{2+} through ferric reductase oxidase (FRO). Subsequently, Fe^{2+} is absorbed by iron regulated transporter (IRT) members (Barton and Abadia 2006; Kobayashi and Nishizawa 2012; Mondal et al. 2022). Strategy II is common in gramineous plants, in which a series of enzymatic reactions are implemented and mugineic acids (MAs) are synthesized and secreted, forming chelates with Fe^{3+} in the rhizosphere. Subsequently, MA-Fe^{3+} chelates are absorbed by the root cells through a specific type of Fe chelator phytosiderophore (PS) pathway that depends on yellow stripe (YS) or yellow stripe-like (YSL) transporters (Schaaf et al. 2005; Zhang et al. 2019; Mondal et al. 2022; Song et al. 2023).

In model plants such as *Arabidopsis* (*Arabidopsis thaliana*) and rice (*Oryza sativa*), IRT1 transporters play a role in root Fe^{2+} transport in Strategy I plants. They also regulate the transport of other ions like Mn^{2+}, Cd^{2+} and Zn^{2+} (Eide et al. 1996; Vert et al. 2002, 2009; Nakanishi et al. 2006; Zelazny and Vert 2015; Fourcroy et al. 2016). AtIRT1 is able to transport a broad range of substrates, including Fe^{2+}, Mn^{2+}, Cd^{2+} and Zn^{2+} (Eide et al. 1996; Roger et al. 2000; Fourcroy et al. 2016). *AtIRT2* was highly expressed in root epidermis, being significantly induced under Fe deficiency. AtIRT2 located in intercellular vesicles stored Fe^{2+} through compartmentalization to prevent excessive accumulation of Fe^{2+} absorbed by AtIRT1 from causing toxicity (Vert et al. 2009; Mondal et al. 2022). IRT1 transporters have been subsequently isolated from *Solanum lycopersicum* (Eckhardt et al. 2001), *Malus xiaojinensis* (Li et al. 2006), and *Arachis hypogaea* (Ding et al. 2010). Notably, rice possesses full Strategy II and partial Strategy I and can directly uptake and utilize Fe^{2+}, depending on the way how it absorbs Fe (Ishimaru et al. 2006; Nakanishi et al. 2006; Kobayashi and Nishizawa 2012; Mondal et al. 2022; Song et al. 2023). In particular, OsIRT1 and OsIRT2 were located in the plasma membrane of root epidermal cells and functioned by transferring Fe^{2+}, similar to that of IRT transporters in Strategy I plants, and can also transport Cd^{2+} (Bughio et al. 2002; Ishimaru et al. 2006; Nakanishi et al. 2006). Further studies revealed that natural resistance associated macrophage proteins (NRAMPs) were identified as a ubiquitous family of metal efflux transporters in rice, and NRAMP1 acts as a transporter of arsenic and manganese and is also essential for low-affinity Fe uptake in rice (Tiwari et al. 2014; Agorio et al. 2017; Mondal et al. 2022; Song et al. 2023).

Application of Fe fertilizer directly influences the growth, flowering, fruit quality, and yield of fruit trees, including grapes (*Vitis vinifera*) (Song et al. 2016a, b, 2023; Sheng et al. 2020). Despite the well-documented genome of grapes (Jaillom et al. 2007), understanding the molecular mechanisms underlying Fe absorption and transport in grape remains limited. In this study, we isolated *VvIRT7* from 'Marselan' grape, exploring its expression pattern and potential biological functions. This study contributes valuable gene resources for unraveling the role of VvIRT transporters in grape, shedding light on the molecular mechanisms of Fe absorption and efficient utilization in fruit trees.

Materials and methods

Plant material and growth condition

This study utilized 5-year-old 'Marselan' vines and 1-month-old tissue-cultured seedlings, sourced from the Shandong Grape Germplasm Repository in Yantai, China (Zhang et al. 2021; Song et al. 2023). The vines and seedlings were grown under controlled conditions in a growth chamber with a 12/12 h day/night light photoperiod, a 25/20 °C day/night thermoperiod, and 60% relative humidity. For sample collection, leaves, stems, and roots of seedlings, as well as young leaves, mature leaves, full-blooming flowers, young fruits, and mature fruits of 5-year-old vines were collected and immediately frozen in liquid nitrogen for subsequent qRT-PCR analysis. Each experiment involved three biological replicates, with 12 sample sections in each.

The 'Marselan' tissue-cultured seedlings were germinated on half-strength MS solid medium (Murashige and Skoog 1962) for 1 month, followed by transfer to half-strength MS solution in plastic containers within the growth chamber. For Fe depletion treatment, Fe was omitted from the MS medium, following established protocols (Song et al. 2014b, 2022, 2023; Zhang et al. 2021). Seedlings underwent Fe depletion for 48 h before expression analysis, and each experiment was replicated three times, with 15 seedlings in each replication.

The wild type *Arabidopsis* (Col-0), the *irt1* knockout mutant, and *irt1*/35S::*IRT7* complementation lines were cultivated in a growth chamber under conditions detailed in previous studies (Zhang et al. 2021; Song et al. 2022, 2023). Seedlings were cultured on half-strength MS medium for 14 days before physiological analysis. The experiments were replicated three times, each involving 20 seedlings.

Physiological analysis

The fresh and dry weights of 20 *Arabidopsis* seedlings (Col-0, *irt1* knockout mutant, and *irt1*/35S::*IRT7* complementation) were measured using an Analytical Balance (Thermo Electron, Waltham, USA). Root characteristics of Col-0, *irt1* knockout mutant, and *irt1*/35S::*IRT7* seedlings, including total root length, lateral root numbers, and total surface area, were analyzed using an Epson Rhizo scanner (Long Beach, CA, USA) and the Epson WinRHIZO software (Long Beach, CA, USA). Fe concentration was determined by ICP-AES systems (IRIS Advantage, Thermo Electron, Waltham, USA)

after samples were digested using the HNO_3–$HClO_4$ method (Song et al. 2014a, 2016b, 2022, 2023; Sheng et al. 2020). Activity assay of aconitase (ACO), nitrite reductase (NiR) and succinate dehydrogenase (SDH) were carried out using relevant detection kits (Nanjing Jiancheng Bioengineering Institute, Nanjing, China), according to the manufacturer's descriptions. Chlorophyll was extracted and quantified using the BioRad SmartSpec 3000 spectrophotometer (Wadsworth, Illinois, USA), as mentioned in Song et al. (2014a, 2022) and Sheng et al. (2020). Chlorophyll extraction and quantification were carried out using the BioRad SmartSpec 3000 spectrophotometer (Wadsworth, Illinois, USA), as detailed in previous studies (Song et al. 2014a, 2016b, 2022, 2023; Sheng et al. 2020).

Tissue Fe distribution analysis

After germination on half-strength MS solid medium for 14 days, *Arabidopsis* seedlings underwent Prussian blue staining following the method outlined by Meguro et al. (2007). Tissue samples were sectioned into small pieces and immersed in a Prussian blue staining solution (4% HCl:4% potassium hexacyanoferrate(II) = 1:1). Subsequently, the stained fragments were washed with deionized water, immersed in chloral hydrate solution until full transparency was achieved, and then subjected to observation using an OLYMPUS CX23 Electron Microscope (Tokyo, Japan). Fe-containing tissues were visualized through a blue stain.

Isolation and cloning of *VvIRT* genes

The putative *VvIRT* genes were identified by referencing the amino acid sequences of *Arabidopsis* AtIRT1-3 (Kobayashi and Nishizawa 2012) and screening the Grape Genome Database (Jaillom et al. 2007). The coding sequence (CDS), genomic DNA sequence, and amino acid sequence of *VvIRT* genes were retrieved. Verification of the amino acid sequences of VvIRT proteins were performed using Pfam and InterProScan 4.8 online servers. Specific prime pairs were designed for CDS cloning of *VvIRT* genes. Total RNA was extracted from 1-month-old 'Marselan' seedlings using the RNAprep Pure Plant Kit (TianGen, Beijing, China), and 1 µg of RNA was reverse-transcribed into the first-strand cDNA template using the PrimeScript™ RT reagent kit (Takara, Dalian, China). The CDS of *VvIRT* genes were then amplified using Prime STARTM HS DNA polymerase (Takara, Dalian, China) and sequenced by Shenggong Bioengineering Co. Ltd. (Shanghai, China). Successfully sequenced CDSs were submitted to NCBI GenBank to obtain accession numbers, which are listed in Supplementary Table S1.

Phylogenetic tree construction

The amino acid sequences of IRT homologs from various plant species, including grape (VvIRT1-VvIRT10), *Arabidopsis thaliana* (AtIRT1-AtIRT3), *Raphanus sativus* (RsIRT1), *Arachis hypogaea* (AhIRT1), *Citrus sinensis* (CsIRT1), *Gossypium hirsutum* (GhIRT1), *Oryza sativa* (OsIRT1 and OsIRT2), *Zea mays* (ZmIRT1), *Populus trichocarpa* (PtIRT1), *Malus xiaojinensis* (MxIRT1), *Prunus persica* (PpIRT1), *P. mume* (PmIRT1), *Pyrus betulaefolia* (PbIRT1), *Solanum lycopersicum* (SlIRT1), and *S. tuberosum* (StIRT1), were aligned using ClusterX 2.0.13 software. The phylogenetic tree of plant IRT homologs was constructed using the maximum likelihood method in MEGA 15.0. A bootstrap test with 1000 iterations was employed to assess the confidence of the tree.

RNA extraction and quantitative real time PCR (qRT-PCR)

Specific primers for *VvIRT* genes were designed using NCBI/Primer-BLAST on-line server (https://www.ncbi.nlm.nih.gov/tools/primer-blast/index.cgi?LINK_LOC=BlastHome). The primer sequences were listed in Supplementary Table S1. PCR analysis was conducted on 7500 Real Time PCR System (Applied Biosystems, New York, USA) using SYBR Premix Ex Taq (TaKaRa, Kyoto, Japan) reaction kit. The specificity of primers was determined by observing the melting curve of qRT-PCR products and the presence of specific bands on agarose gel. The grape in-house keeping gene *Ubiquitin* was used as the internal reference for normalization, as in previous studies (Tang et al. 2020; Zhang et al. 2021; Song et al. 2023). PCR conditions were arranged as follows: 95 °C for 30 s, 40 cycles of 95 °C for 5 s, and 60 °C for 34 s. Relative expression levels of *VvIRT* genes were presented after normalization to the internal reference *Ubiquitin* from three independent biological repeats, each with four technical replicates.

To investigate the response of *VvIRT* genes under Fe depletion at the transcriptional level, the expression value under control condition was set as 1. A relative expression value under Fe depletion < 1 indicates a decrease in the gene expression level (depicted in blue), while a value > 1 it means an increase in the gene expression level (depicted in red). A heat map illustrating the expression changes was generated using HemI software (Sheng et al. 2020; Zhang et al. 2021, 2022; Song et al. 2022, 2023).

Complementation of *VvIRT7* gene in yeast mutant

The recombinant plasmid pYH23-*IRT7* was constructed by cloning the CDS region of *VvIRT7* gene into pYH23 vector (Eide et al. 1996; Nakanishi et al. 2006; Vert et al. 2009),

using the forward primer 5′- GACGGATCCATGGCC TCGTGCGTAGGCGAT -3′ (*BamH* I was underlined) and reverse primer 5′- GAGTCTAGAGTCAGGCCCAAAGGG CCAGAAC -3′ (*Xba* I was underlined). According to the description of Eide et al. (1996) and Vert et al. (2009), yeast mutant DEY1453 (*MAT α/MAT α Ade2/+canl/canl his3/his3 leu2/leu2 trpl/trpl ura3/ura3 fet3-2*::*HIS3/fet3-2*::*HIS3fet4-1*::*LEU2/fet4-1*::*LEU2*) was transformed with pYH23 or recombinant plasmid pYH23-*IRT7*. Yeast transformants were cultured in liquid YPD medium (1% yeast extract, 2% peptone, 2% glucose) until the OD_{600} reached 1.0. The culture was then diluted to concentrations of 10^{-1}, 10^{-2}, and 10^{-3}. Yeast cell growth was determined in synthetic defined medium (SD, 6.7 g L^{-1} of yeast nitrogen base without amino acids, pH 5.5), supplied with 10 or 0 μmol L^{-1} Fe_2SO_4, respectively. For Fe-depleted media (0 μmol L^{-1} Fe_2SO_4), 50 μmol L^{-1} bathophenanthroline disulfonic acid (BPDS) was added. Pictures were taken 60 h after incubation at 30 °C.

Generation of transgenic *Arabidopsis* complementing *VvIRT7* gene

The recombinant plasmid pBH-*IRT7* was constructed by cloning the CDS region of *VvIRT7* gene into pBH vector (Supplementary Fig. S1; Song et al. 2022; Zhang et al. 2022), using the forward primer 5′- GACGAGCTCATG GCCTCGTGCGTAGGCGAT -3′ (*Sac*I was underlined) and reverse primer 5′- GAGTCTAGATCAGGCCCAAAG GGCCAGAAC -3′ (*Xba* I was underlined). The recombinant plasmid was subcloned into *Agrobacterium tumefaciens* EHA 105. Subsequently, it was transformed into the previously germinated *Arabidopsis irt1* knockout homozygote mutant on half-strength MS solid medium for 1 month, using the floral dip method. Independent T1 generation of *irt1*/35S::*IRT7* complementation lines were obtained by screening hygromycin resistant regenerated *Arabidopsis* seedlings. The genomic DNA was extracted from T1 generation of *irt1*/35S::*IRT7* lines using the Universal Genomic DNA Extraction Kit (TaKaRa, Dalian, China), and further verified the existence of a 1008 bp product of *VvIRT7* by reverse transcription PCR. T1 generation of *irt1*/35S::*IRT7* seedlings were grown on half-strength MS solid medium for 2 weeks, and total RNA of shoots and roots T1 transgenic lines were extracted and synthesized into the first strand cDNA template for presence determination of *VvIRT7*. Purified T3 generation seeds of #1, #5, and #15 *irt1*/35S::*IRT7* complementation lines were harvested and sown on half-strength MS solid medium for 21 days before physiological analysis, respectively. Data of #1 *irt1*/35S::*IRT7* complementation lines were shown in this work. Biological repeats were carried out for three times, each with 20 seedlings.

Statistical analysis

Graphs were created using Origin 12.0 software. Significant differences were analyzed using the Student's *t*-test in SPSS 13.0 software (SPSS Chicago, IL, USA) or ANOVA followed by Fisher's LSD test, with details provided in the legends.

Results

Isolation of IRT genes in grape

In total, 10 putative *IRT* genes were identified from the grape genome and designated as *VvIRT1* to *VvIRT10* (see Supplementary Fig. S2). The Genbank numbers of these genes are listed in Supplementary Table S1. Protein domain verification demonstrated that all of them possess the zinc/Fe transporter domain (PF02535), confirming their classification as Fe regulated transporters.

Phylogenetic tree analysis revealed that IRT homologs from Rosaceae (*M. xiaojinensis*, *P. betulaefolia*, *P. persica*, and *P. mume*), Gramineae (*O. sativa* and *Z. mays*) or Brassicaceae (*A. thaliana* and *R. sativus*) share the closest genetic relationships. Moreover, VvIRT1 was closely clustered with known plant IRT1 homologs, including AtIRT1, SlIRT1, and Rosaceae IRT1 members. VvIRT2 and VvIRT3 were tightly clustered with OsIRT1 and ZmIRT1, while VvIRT4-10 transporters were prone to be closely clustered together (Fig. 1).

Expression profiles of *VvIRT* genes

Results showed that the expression levels of *VvIRT* genes varied significantly among different tested tissues/organs, including annual young leaves, mature leaves, new phloem, new roots, full blooming flowers, young fruits, mature fruits, and leaves, stems, and roots of 'Marselan' seedlings (Fig. 2). In particular, the overall expression of *VvIRT7* was the most abundant, with the highest level observed in roots (both in adult vines and seedlings), followed by mature fruits and leaves (in both adult vines and seedlings). Notably, *VvIRT8* exhibited specific expression in full bloom flowers, and *VvIRT9* was dominantly expressed in leaves, while *VvIRT1* and *VvIRT2* were exclusively observed in roots of both adult vines and seedlings. Additionally, the highest expression level of *VvIRT6* were found in mature fruits, followed by leaves. Although the overall expression level was extremely low, the highest expression level of *VvIRT4* was detected in roots, and *VvIRT5* showed the highest expression in fruits. However,

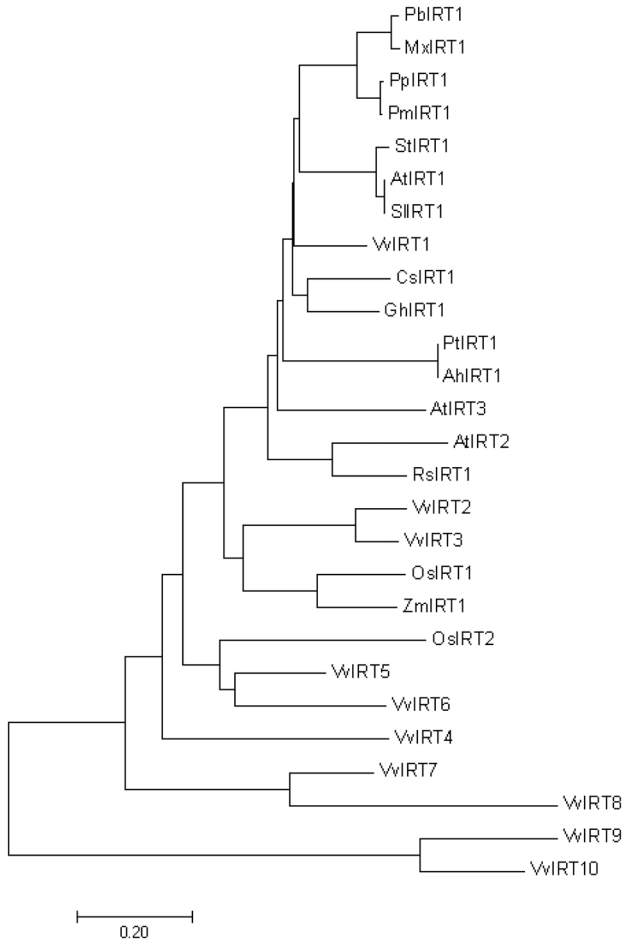

Fig. 1 Phylogenetic tree of plant IRT homologs. Phylogenetic tree of plant IRT homologs from grape (VvIRT1-VvIRT10), *Arabidopsis thaliana* (AtIRT1-AtIRT3), *Raphanus sativus* (RsIRT1), *Arachis hypogaea* (AhIRT1), *Citrus sinensis* (CsIRT1), *Gossypium hirsutum* (GhIRT1), *Oryza sativa* (OsIRT1 and OsIRT2), *Zea mays* (ZmIRT1), *Populus trichocarpa* (PtIRT1), *Malus xiaojinensis* (MxIRT1), *Prunus persica* (PpIRT1), *P. mume* (PmIRT1), *Pyrus betulaefolia* (PbIRT1), *Solanum lycopersicum* (SlIRT1), and *S. tuberosum* (StIRT1) was constructed using the maximum likelihood method in MEGA 13.0 to analyze the genetic evolution relationship. Scale indicates genetic distance

the expression of *VvIRT3* and *VvIRT10* was not detected in the tested tissues in this study (Fig. 2).

Differential response of *VvIRT* genes under Fe depletion in tissue-cultured seedlings

Further analysis revealed that *VvIRT* genes exhibited differential responses to Fe depletion in tissue-cultured grape seedlings (Fig. 3). Thus, five genes (*VvIRT1*, *VvIRT4*, *VvIRT6*, *VvIRT7* and *VvIRT9*) responded to Fe depletion in at least one tested tissue (leaves, stems, or roots), showing significantly increased expression levels, while the remaining five genes exhibited minimal changes. Notably, *VvIRT4*, *VvIRT6*, and *VvIRT7* demonstrated high sensitivity to Fe depletion, with their expression levels up-regulated throughout the entire plant seedlings. Additionally, the expression of *VvIRT1* and *VvIRT9* in roots was induced under Fe depletion (Fig. 3).

VvIRT7 restored the normal growth of yeast mutant DEY1453

Given that *VvIRT7* emerged as the most abundantly expressed gene in the *IRT* family of grapes, particularly in roots, with heightened expression under Fe depletion across all tested tissues (Figs. 2, 3), we proceeded to functionally assess VvIRT7 using yeast expression system. The yeast mutant DEY1453, which is deficient in Fe^{2+} uptake, cannot grow normally on YPD medium in the absence of Fe^{2+} (Eide et al. 1996; Nakanishi et al. 2006; Vert et al. 2009). We conducted a comparison of yeast cell growth on YPD medium supplemented with varying concentrations of Fe^{2+}. Notably, DEY1453 cells harboring either pYH23 or pYH23-*IRT7* thrived on YPD medium supplemented with 10 µmol L^{-1} Fe^{2+}. However, only DEY1453 cells containing pYH23-*IRT7* displayed normal growth on YPD medium supplemented with 0 µmol L^{-1} Fe_2SO_4, while DEY1453 cells with the empty vector pYH23 failed to grow (Fig. 4). These findings suggest that VvIRT7 directly participates in Fe^{2+} uptake or transport in yeast, thereby restoring the normal growth of the DEY1453 mutant.

VvIRT7 rescued the retarded growth of *Arabidopsis irt1* mutant

In *Arabidopsis*, the growth of the *irt1* knockout mutant was severely hindered, accompanied with chlorosis symptoms (Eide et al. 1996; Vert et al. 2002, 2009). To investigate whether *VvIRT7* could restore the normal growth of the *irt1* mutant, *VvIRT7* was subcloned into the binary expression vector pHB (Supplementary Fig. S1A). At least 6 putativeT1 generation *irt1*/35S::*IRT7* complementation lines (#1, #5, #7, #11, #12, and #15) were verified using reverse transcription PCR for the presence of a 1008 kb fragment of *VvIRT7* (Supplementary Fig. S1B), which was dominantly expressed in the roots of T1 generation *irt1*/35S::*IRT7* lines (Fig. 5A). Purified T3 generation of #1, #5, and #15 *irt1*/35S::*IRT7* lines were randomly selected for further physiological analysis, with data of #1 *irt1*/35S::*IRT7* lines presented in this work.

Compared to the wild type, the *irt1* mutant lines exhibited severe withering, loss of green leaves, and reduced fresh weight, dry weight, total root length, total root surface, lateral root numbers, and total leaf chlorophyll under both control conditions and Fe depletion (Fig. 5B; Table 1). Indeed, the tissue Fe concentration in *irt1* mutant lines was

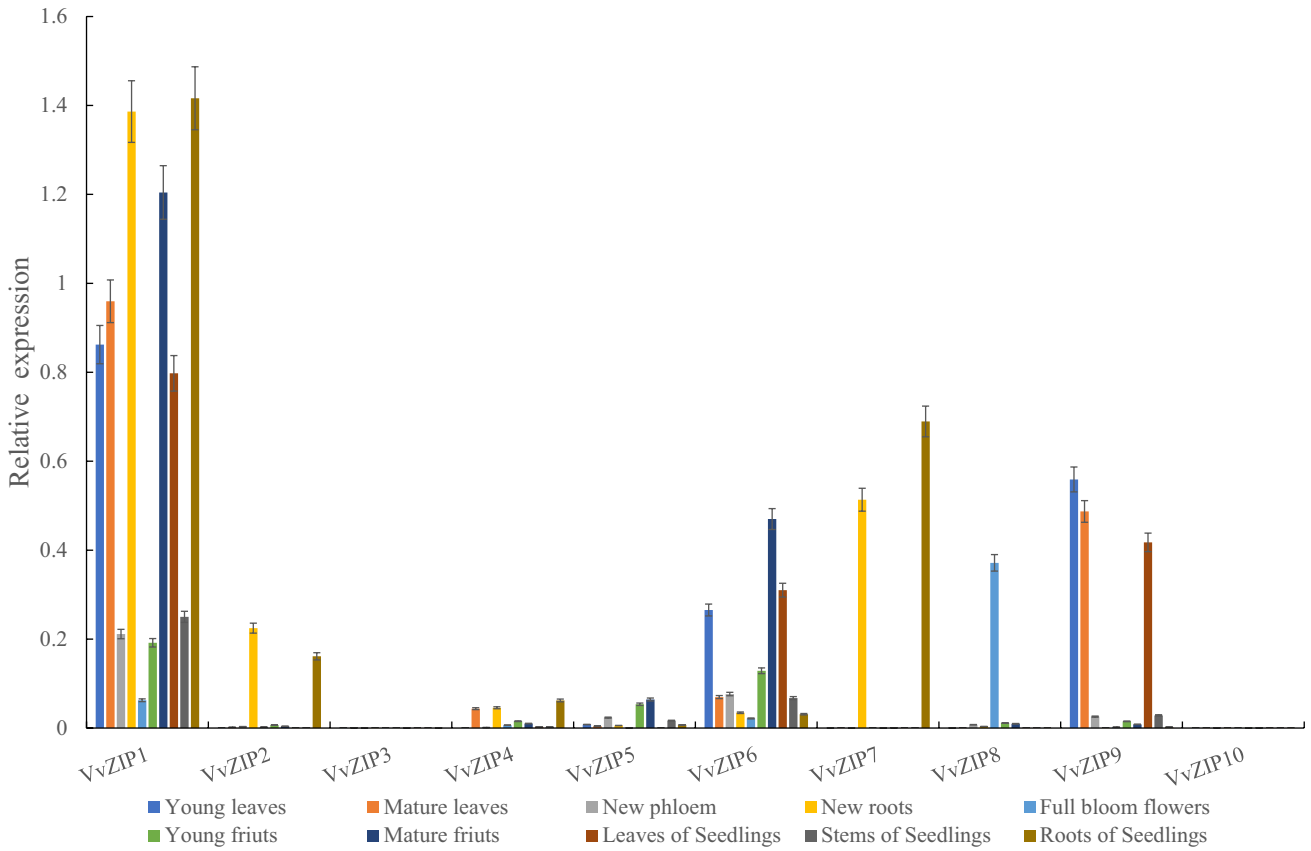

Fig. 2 Tissue specific expression analysis of *VvIRT* genes in grape. Samples of leaves, stems and roots of seedlings, and young leaves, mature leaves, full blooming flowers, young fruits, and mature fruits of 5-year-old vines were collected and frozen immediately in liquid nitrogen before qRT-PCR analysis. Data are presented as means ± SD (n = 3)

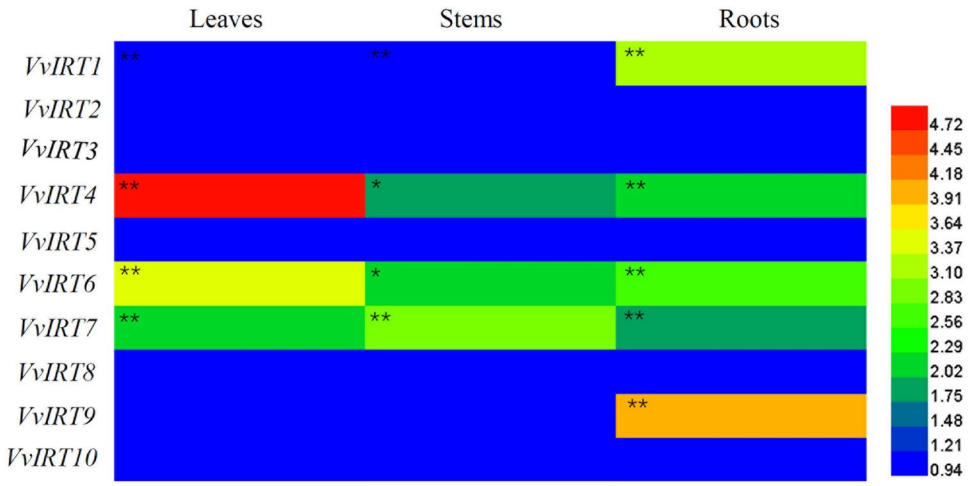

Fig. 3 Response of *VvIRT* genes to Fe depletion in grape seedlings. One-month-old tissue-cultured 'Marselan' seedlings were subjected to Fe depletion for 48 h before analysis. Relative expression levels of the target genes were normalized to the internal control (*Ubiquitin*) from three independent biological replicates. Data are presented as means ± SD (n = 3). Significant differences between control and Fe-depleted conditions at $P \leq 0.05$ were determined using Student's *t*-test in the SPSS 13.0 software

significantly reduced under both conditions (Table 1). Notably, the Fe–S protein NiR, a key enzyme in chloroplastic nitrogen assimilation, as well as ACO and SDH, crucial for mitochondrial citric acid cycle of glycol metabolism, showed significantly reduced activity in *irt1* mutant lines under both conditions (Table 1). In contrast, #1 *irt1*/35S::*IRT7* lines exhibited a healthier growth status than that of the *irt1* mutant lines under both conditions (Fig. 5B). Simultaneously, the fresh weight, dry weight, total root length, total root surface, lateral root numbers, total leaf chlorophyll, ACO activity, NiR activity, and SDH activity of #1 *irt1*/35S::*IRT7* lines were significantly enhanced, compared

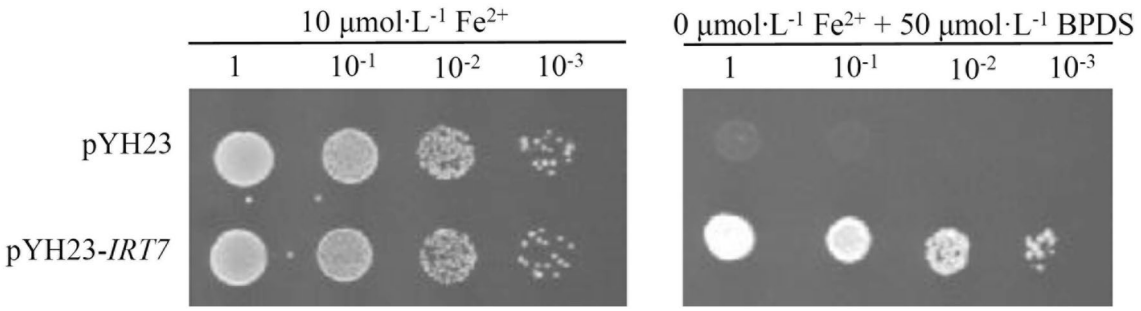

Fig. 4 Functional determination of *VvIRT7* in yeast. The yeast mutant DEY1453, harboring either the empty vector pYH23 or the recombinant plasmid pYH23-*IRT7*, was cultured in liquid YPD medium (1% yeast extract, 2% peptone, 2% glucose) until reaching an OD_{600} of 1.0. The culture was then diluted to concentrations of 10^{-1}, 10^{-2}, and 10^{-3}. Yeast cell growth was assessed in synthetic defined medium (6.7 g L^{-1} of yeast nitrogen base without amino acids, pH 5.5) supplemented with either 10 or 0 μmol L^{-1} Fe_2SO_4. For Fe-depleted media (0 μmol L^{-1} Fe_2SO_4), 50 μmol L^{-1} bathophenanthroline disulfonic acid (BPDS) was added. Pictures were captured after 60 h of incubation at 30 °C

to the *irt1* mutant (Table 1). These findings imply that the complementation of *VvIRT7* effectively rescued the retarded growth of the *irt1* mutant.

In comparison to the wild type, the tissue Fe concentration in the whole plant of *irt1* mutant lines decreased under both control conditions and Fe depletion. Conversely, the Fe concentration in *irt1*/35S::*IRT7* lines was increased compared to that of the *irt1* mutant lines. Consistently, under control conditions, tissue Prussian blue staining analysis revealed that the most abundant Fe was detected in the roots of the wild type, while tissue Fe distribution was significantly reduced in tested tissues of *irt1* mutants (Fig. 6). Notably, Fe distribution was specifically strengthened in the roots of #1 *irt1*/35S::*IRT7* lines compared to that of *irt1* mutants (Fig. 6), which aligns with the fact that *VvIRT7* was dominantly expressed in the roots the of the T1 generation *irt1*/35S::*IRT7* lines (Fig. 5A). However, Fe distribution was hardly observed in all tested seedlings under Fe depletion, and there was no significant difference among the wild type, *irt1* mutant, and #1 *irt1*/35S::*IRT7* lines (Supplementary Fig. S3). These findings collectively suggest that the iron regulated transporter VvIRT7 is likely implicated in regulating Fe^{2+} transport in grape.

Discussion

As one of the most indispensable mineral elements in fruit trees, Fe directly affects tree growth, flowering, fruit quality formation, and fruit yield (Couturier et al. 2013; Song et al. 2016a, b, 2022, 2023; Sheng et al. 2020). The concentration of Fe required for normal plant growth is typically in the range of 10^{-9} to 10^{-4} mol L^{-1}. However, the concentration of Fe^{2+} and Fe^{3+} in soils under normal pH values usually does not exceed 10^{-15} mol L^{-1}, falling significantly short of meeting the needs for normal plant growth (Barton and Abadia 2006; Kobayashi and Nishizawa 2012; Couturier et al. 2013). Despite the critical role of Fe, the molecular basis and regulatory mechanisms governing Fe uptake and transport in fruit trees remain largely unknown. As a dicotyledon woody fruit vine, grape belongs to Strategy I Fe absorption plants (Kobayashi and Nishizawa 2012; Zhang et al. 2019; Mondal et al. 2022). In this study, we isolated 10 VvIRT transporters from grapes, and the corresponding amino acid sequences, along with homologs from 14 other plants, were highly conserved, with an identity of 60.58% (Supplementary Fig. S1). Notably, IRT homologs of Rosaceae, Cruciferous, or Gramineae were prone to be closely clustered, while VvIRT transporters were likely to be tightly clustered (Fig. 1), implying that IRT homologs from the same family or near genus may possess a closer genetic distance and similar biological functions during the long-term evolution. Therefore, studying the function of grape IRT transporters may provide theoretical support for revealing the biological function of IRT homologs from *Vitaceae* or *Vitis* plants.

In particular, four genes (*VvIRT1*, *VvIRT2*, *VvIRT4* and *VvIRT7*) exhibit high expression levels in the roots of both adult vines and tissue cultured seedlings (Fig. 2), which aligns with observations in other plant species such as *AtIRT1* and *AtIRT2* in *Arabidopsis* (Eide et al. 1996; Vert et al. 2002, 2009), *OsIRT1* and *OsIRT2* in rice (Ishimaru et al. 2006; Nakanishi et al. 2006), *AhIRT1* in peanut (Ding et al. 2010), *MxIRT1* in *M. xiaojinensis* (Li et al. 2006), and *RsIRT1* in radish (He et al. 2013), suggesting a functional role for IRT transporters in plant roots. Previously studies demonstrated that the expression of *AtIRT1* (Eide et al. 1996), *AhIRT1* (Ding et al. 2010), *MxIRT1* (Li et al. 2006), and *RsIRT1* (He et al. 2013) in roots significantly increased under Fe depletion. Consistently, 5 out of 10 genes (*VvIRT1*, *VvIRT4*, *VvIRT6*, *VvIRT7* and *VvIRT9*) were responsive to Fe depletion in grape, with their expression significantly

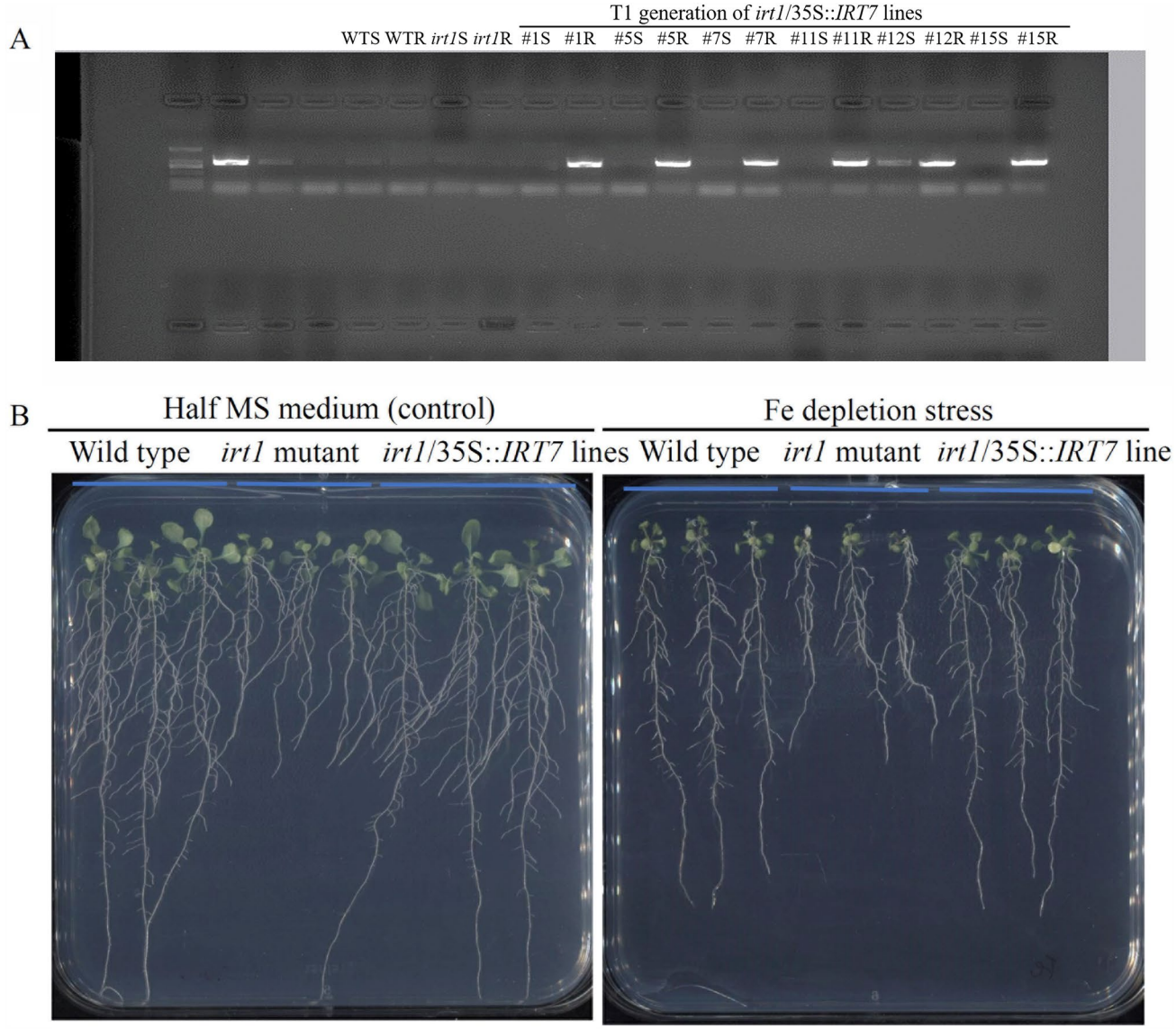

Fig. 5 Generation and phenotype analysis of *VvIRT7* complementation *Arabidopsis* seedlings. **A** Tissue specific expression of *VvIRT7* in T1 generation *irt1*/35S::*IRT7* lines. The genomic DNA was extracted from T1 generation of *irt1*/35S::*IRT7* lines using the Universal Genomic DNA Extraction Kit (TaKaRa, Dalian, China) and further verified for the existence of a 1008 bp product of *VvIRT7* by reverse transcription PCR. **B** Phenotype analysis of T3 generation #1 *irt1*/35S::*IRT7* lines. *Arabidopsis* seedlings were grown on half-strength MS solid medium for 14 days before phenotype analysis. The control condition is shown on the left, and Fe depletion condition is shown on the right. *Note* M, standard DL2000 DNA ladder (Takara, Dalian, China). *WT* wild type, *S* shoots, *R* roots. (Color figure online)

up-regulated, particularly in roots (Fig. 3). These findings suggest that these *IRT* genes play a crucial role in ensuring Fe uptake/transport in grape under Fe depletion, thereby maintaining optimal Fe^{2+} uptake or transport capacity in limited Fe conditions to support essential life activities dependent on Fe. Notably, *VvIRT3* and *VvIRT10* were not detected in the tested tissues in this study, potentially due to the higher threshold in the qRT-PCR identification system. Simultaneously, these two genes are likely to be pseudogenes that may have lost their protein-coding ability due to accumulated mutations or unprocessed segmental duplication over long-term evolution (Li et al. 2013; Cheetham et al. 2019), requiring further verification. Furthermore, the highest expression level of *VvIRT7* was observed in roots, being 3–30 times that of *VvIRT1*, *VvIRT4*, *VvIRT6*, and *VvIRT9* genes, respectively (Fig. 2). We speculate that the abrupt increase in *VvIRT7* expression may serve as a crucial indicator that grape vines respond to environmental Fe deficiency stresses.

In *Arabidopsis*, *AtIRT1* was identified as a key player in Fe^{2+} transport and the maintenance of cation dynamic equilibrium, with the knockout severely impeding normal

Table 1 Physiological analysis of *irt1*/35S::*IRT7* lines under control conditions

Items	Treatment	Wild type	*irt1* mutant	#1 *irt1*/35S::*IRT7* lines
Fresh weight (g)	Control	$0.62 \pm 0.02^{a(a)}$	$0.27 \pm 0.02^{b(a)}$	$0.59 \pm 0.04^{a(a)}$
	Fe depletion	$0.21 \pm 0.03^{a(b)}$	$0.08 \pm 0.007^{b(b)}$	$0.19 \pm 0.02^{a(b)}$
Dry weight (g)	Control	$0.06 \pm 0.005^{a(a)}$	$0.03 \pm 0.002^{b(a)}$	$0.05 \pm 0.003^{a(a)}$
	Fe depletion	$0.02 \pm 0.001^{a(b)}$	$0.01 \pm 0.001^{b(b)}$	$0.02 \pm 0.002^{a(b)}$
Total root length (m)	Control	$14.41 \pm 1.02^{a(a)}$	$3.92 \pm 0.037^{b(a)}$	$14.36 \pm 1.36^{a(a)}$
	Fe depletion	$3.29 \pm 0.31^{a(b)}$	$1.89 \pm 0.22^{b(b)}$	$3.22 \pm 0.29^{a(b)}$
Total surface area (m^2)	Control	$0.48 \pm 0.05^{a(a)}$	$0.15 \pm 0.02^{b(a)}$	$0.51 \pm 0.042^{a(a)}$
	Fe depletion	$0.11 \pm 0.01^{a(b)}$	$0.04 \pm 0.004^{b(b)}$	$0.12 \pm 0.01^{a(b)}$
Lateral root numbers	Control	$363 \pm 21^{a(a)}$	$125 \pm 15^{b(a)}$	$357 \pm 24^{a(a)}$
	Fe depletion	$401 \pm 23^{a(a)}$	$134 \pm 18^{b(a)}$	$389 \pm 23^{a(a)}$
Leaf total chlorophyll (g kg^{-1} FW)	Control	$1.77 \pm 0.20^{a(a)}$	$1.15 \pm 0.057^{b(a)}$	$1.69 \pm 0.11^{a(a)}$
	Fe depletion	$0.82 \pm 0.01^{a(b)}$	$0.39 \pm 0.04^{b(b)}$	$0.78 \pm 0.07^{a(b)}$
ACO activity [U (mg protein)$^{-1}$]	Control	$0.85 \pm 0.09^{a(a)}$	$0.59 \pm 0.05^{b(a)}$	$0.79 \pm 0.06^{a(a)}$
	Fe depletion	$0.49 \pm 0.04^{a(b)}$	$0.33 \pm 0.02^{b(b)}$	$0.44 \pm 0.04^{a(b)}$
NiR activity [U (mg protein)$^{-1}$]	Control	$3.68 \pm 0.32^{a(a)}$	$1.91 \pm 0.17^{b(a)}$	$3.32 \pm 0.22^{a(a)}$
	Fe depletion	$2.42 \pm 0.22^{a(b)}$	$1.30 \pm 0.12^{b(b)}$	$2.33 \pm 0.21^{a(b)}$
SDH activity [U (mg protein)$^{-1}$]	Control	$9.79 \pm 0.94^{a(a)}$	$6.38 \pm 0.45^{b(a)}$	$9.31 \pm 0.76^{a(a)}$
	Fe depletion	$6.47 \pm 0.59^{a(b)}$	$4.36 \pm 0.42^{b(b)}$	$6.12 \pm 0.51^{a(b)}$
Fe concentration (g kg^{-1} DW)	Control	$0.13 \pm 0.01^{a(a)}$	$0.079 \pm 0.006^{b(a)}$	$0.12 \pm 0.01^{a(a)}$
	Fe depletion	$0.021 \pm 0.002^{b(a)}$	$0.013 \pm 0.001^{b(b)}$	$0.019 \pm 0.002^{a(b)}$

Note Seedlings of wild type, *irt1* mutant and T3 generation *irt1*/35S::*IRT7* lines were germinated on half-strength MS (control) or Fe depletion solid medium, respectively, for 14 days before physiological analysis. Data are presented as means ± SD (n = 3). Letters represent significant differences at $P \leq 0.05$ as determined using ANOVA followed by Fisher's LSD test. Letters outside the parentheses indicate differences among the wild type, mutant and complementation lines and those inside the parentheses indicate differences between the control condition and Fe depletion

ACO aconitase, *DW* dry weight, *Fe* iron, *FW* fresh weight, *NiR* nitrite reductase, *SDH* succinate dehydrogenase

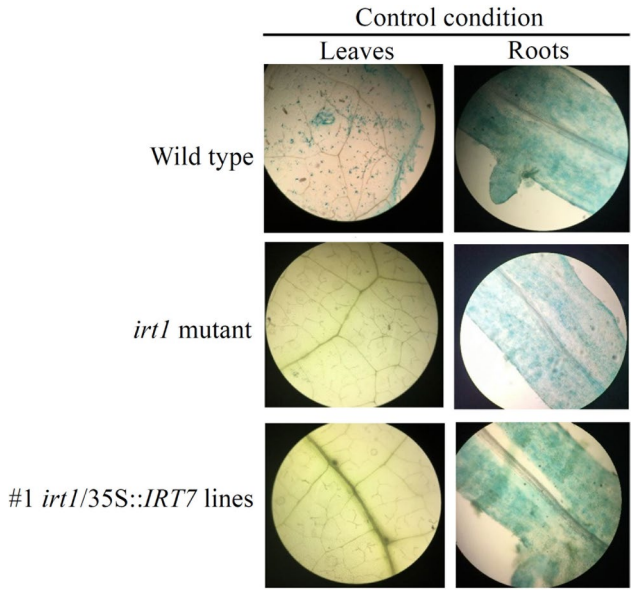

Fig. 6 Tissue Fe distribution analysis. After germination on half-strength MS solid medium for 14 days, *Arabidopsis* seedlings were subjected to Prussian blue staining, and sliced tissue sections were chosen for microscope examination of tissue iron distribution. Fe-containing tissues were dyed in blue. (Color figure online)

plant growth (Eide et al. 1996). Despite having lower similarity to AtIRT1 (compared to VvIRT1, VvIRT2, or VvIRT3), *VvIRT7* stands out as the most abundantly expressed IRT gene in grapes, exhibiting an increase in all tested tissues under Fe depletion. Moreover, the overexpression of *VvIRT7* successfully rescued an *Arabidopsis irt1* mutant in this study, potentially linked to distinct protein expression levels resulting from amino acid sequence divergence (Supplementary Fig. S2). Notably, the maximum expression level of *VvIRT7* was detected in roots, three times that of *VvIRT1* and six times that of *VvIRT3*. Despite being controlled by of a constitutive 35S promoter rather than its intrinsic promoter, the expression of *VvIRT7* in transgenic *Arabidopsis* lines is higher in roots than in shoots (Fig. 5A). The site of integration of the transgene (*VvIRT7*) into the *Arabidopsis irt1* mutant genome can influence its expression, and the 35S promoter may undergo epigenetic modifications in the roots of the transgenic lines, leading to its preferential silencing or activation in these tissues. Nonetheless, these findings partially explain that overexpression of *VvIRT7* explain the specific strengthening of Fe distribution in the roots of *irt1*/35S::*IRT7* lines, as revealed by further tissue Prussian

blue staining, with the most abundant Fe detected in the roots of the wild type.

Encouragingly, tissue Fe concentration significantly increased in *irt1*/35S::*IRT7*, partially explaining the improved growth performance. Complementation of *VvIRT7* may actively mobilize the limited Fe uptake capacity of *irt1*/35S::*IRT7* lines to maintain basic life activities and metabolic processes dependent on a sufficient amount of Fe, including chlorophyll synthesis and the activities of key Fe–S proteins. Indeed, total leaf chlorophyll and the activities of ACO, NiR, and SDH were synchronously enhanced in *irt1*/35S::*IRT7* lines (Table 1), contributing beneficially to plant perseverance. Once again, these findings underscore the indispensable role of Fe as a mineral element for plants to maintain normal growth (Barton and Abadia 2006; Couturier et al. 2013; Song et al. 2016a, b, 2022). Nonetheless, VvIRT7 emerges as a crucial Fe-regulated transporter implicated in root Fe^{2+} uptake or transport in grapes, especially under Fe-deficient conditions.

Conclusion

In summary, we isolated a total of 10 *VvIRT* family genes in grapes, revealing significant differences in their expression levels across distinct grape tissues and organs. *VvIRT7*, identified as the most abundantly expressed IRT family gene in grapes, demonstrated a remarkable ability to transport Fe^{2+}, successfully restoring normal growth in the DEY1453 mutant. Furthermore, the overexpression of *VvIRT7* proved effective in rescuing the impaired growth of the *Arabidopsis irt1* knockout mutant.

Supplementary Information The online version contains supplementary material available at https://doi.org/10.1007/s11240-023-02624-1.

Acknowledgements The authors are grateful to grateful to Professor Julia M. Davies, Department of Plant Sciences, University of Cambridge for critical reading and valuable suggestions. This work has been jointly supported by the following grants: The Major Project of Science and Technology of Shandong Province (2022CXGC010605), the China Agriculture Research System of MOF and MARA (CARS-29-17), the China Scholarship Council Fund (202208370080), and Yantai K&R Project (2020XCZX026).

Author contributions ZS, BP and MT conceived and designed the experiments. BP, XW, ML, SS, and GY performed the experiments. YN and HZ analyzed the data. ZS and MT wrote the manuscript. ZS, GY, and YN revised the manuscript. All authors have read and approved the final manuscript.

Funding Major Project of Science and Technology of Shandong Province, 2022CXGC010605, Meiling Tang; China Agriculture Research System of MOF and MARA, CARS-29-17, Meiling Tang; China Scholarship Council Fund, 202208370080, Zhizhong Song; Yantai K&R Project, 2020XCZX026, Bin Peng.

Data availability All data supporting the findings of this study are available within the paper and within its supplementary materials published online.

Declarations

Conflict of interest We declare that we do not have any commercial or associative interest that represents a conflict of interest in connection with the work submitted.

References

Agorio A, Giraudat J, Bianchi MW, Marion J, Espagne C, Castaings L, Lelièvre F, Curie C, Thomine S, Merlot S (2017) Phosphatidylinositol 3-phosphate-binding protein AtPH1 controls the localization of the metal transporter NRAMP1 in *Arabidopsis*. Proc Natl Acad Sci USA 114:E3354–E3363

Barton LL, Abadia J (2006) Iron nutrition in plants and rhizospheric microorganisms. Springer, Netherlands, Dordrecht, pp 85–101

Bughio N, Yamaguchi H, Nishizawa NK, Nakanishi H, Mori S (2002) Cloning an iron-regulated metal transporter from rice. J Exp Bot 53:1677–1682

Cheetham SW, Faulkner GJ, Dinger ME (2019) Overcoming challenges and dogmas to understand the functions of pseudogenes. Nat Rev Genet 21:191–201

Couturier J, Touraine B, Briat JF, Gaymard F, Rouhier N (2013) The iron-sulfur cluster assembly machineries in plants: current knowledge and open questions. Front Plant Sci 4:259

Ding H, Duan LH, Li J, Yan HF, Zhao M, Zhang FS, Li WX (2010) Cloning and functional analysis of the peanut iron transporter AhIRT1 during iron deficiency stress and intercropping with maize. J Plant Physiol 167(12):996–1002

Eckhardt U, Marques AM, Buckhout TJ (2001) Two iron-regulated cation transporters from tomato complement metal uptake-deficient yeast mutants. Plant Mol Biol 45:437–448

Eide D, Broderius M, Fett J, Guerinot ML (1996) A novel iron-regulated metal transporter from plants identified by functional expression in yeast. Proc Natl Acad Sci USA 93(11):5624–5628

Fourcroy P, Tissot N, Gaymard F, Briat JF, Dubos C (2016) Facilitated Fe nutrition by phenolic compounds excreted by the *Arabidopsis* ABCG37/PDR9 transporter requires the IRT1/FRO2 high-affinity root Fe(2+) transport system. Mol Plant 9(3):485–488

He XY, Gong YQ, Xu L, Lai DQ, Wen TC, Liu LW (2013) Molecular characterization of iron-regulated transporter gene *RsIRT1* in radish. J Nanjing Agric Univ 36(6):13–18 (**in Chinese**)

Ishimaru Y, Suzuki M, Tsukamoto T, Suzuki K, Nakazono M, Kobayashi T, Wad Y, Watanabe S, Matsuhashi S, Takahashi M, Nakanishi H, Mori S, Nishizawa NK (2006) Rice plants take up iron as an Fe^{3+}-phytosiderophore and as Fe^{2+}. Plant J 45(3):335–346

Jaillon O, Aury JM, Noel B, Policriti A, Clepet C, Casagrabde A, Choisne N, Aubourg S, Vitulo N, Jubin C, Vezzi A, Legeai F, Hugueney P, Dasilva C, Horner D, Mica E, Jublot D, Poulain J, Bruyère C, Billault A, Segurens B, Gouyvenoux M, Ugarte R, Cattonaro F, Anthouard V, Vico V, Del Fabbro C, Alaux M, Di Gaspero G, Dumas V, Felice N, Paillard S, Juman I, Moroldo M, Scalabrin S, Canaguier A, Le Clainche I, Malacrida G, Durand E, Pesole G, Laucou V, Chatelet P, Merdinoglu D, Delledonne M, Pezzotti M, Lecharny A, Scarpelli C, Artiguenave F, Pèm E, Valle G, Morgante M, Caboche M, Adam-Blondon AF, Weissenbach J, Quétier F, Wincker P (2007) The grapevine genome sequence suggests ancestral hexaploidization in major angiosperm phyla. Nature 449(7161):463–467

Kobayashi T, Nishizawa NK (2012) Iron uptake, translocation, and regulation in higher plants. Annu Rev Plant Biol 63:131–152

Li P, Qi JL, Wang L, Huang QN, Han ZH, Yin LP (2006) Functional expression of *MxIRT1*, from *Malus xiaojinensis*, complements an iron uptake deficient yeast mutant for plasma membrane targeting via membrane vesicles trafficking process. Plant Sci 171:52–59

Li W, Yang W, Wang XJ (2013) Pseudogenes: pseudo or real functional elements? J Genet Genomics 40(4):171–177

Lill R (2009) Function and biogenesis of iron-sulphur proteins. Nature 460:831–838

Meguro R, Asano Y, Odagiri S, Li C, Iwatsuki H, Shoumura K (2007) Nonheme-iron histochemistry for light and electron microscopy: a historical, theoretical and technical review. Arch Histol Cytol 70:1–19

Mondal S, Pramanik K, Ghosh SK, Pal P, Ghosh PK, Ghosh A, Maiti TK (2022) Molecular insight into arsenic uptake, transport, phytotoxicity, and defense responses in plants: a critical review. Planta 255:87

Murashige T, Skoog F (1962) A revised medium for rapid growth and bioassays with tobacco tissue cultures. Physiol Plant 15:473–497

Nakanishi H, Ogawa I, Ishimaru Y, Mori S, Nishizawa NK (2006) Iron deficiency enhances cadmium uptake and translocation mediated by the Fe^{2+} transporters OsIRT1 and OsIRT2 in rice. Soil Sci Plant Nutr 52:464–469

Roger E, Eide DJ, Guerinot ML (2000) Altered selectivity in an *Arabidopsis* metal transporter. Proc Natl Acad Sci USA 97:12356–12360

Schaaf G, Häberle J, von Wirén N, Schikora A, Curie C, Vert G, Briat JF, Ludewig UA (2005) Putative function for the *Arabidopsis* Fe-phytosiderophore transporter homolog AtYSL2 in Fe and Zn homeostasis. Plant Cell Physiol 46:762–774

Sheng YT, Cheng H, Wang LM, Shen JY, Tang ML, Liang MX, Zhang K, Zhang HX, Kong Q, Yu ML, Song ZZ (2020) Foliar spraying with compound amino acid-iron fertilizer increases leaf fresh weight, photosynthesis and Fe-S cluster gene expression in peach [*Prunus persica* (L.) Batsch]. Biomed Res Int 2020:2854795

Song ZZ, Yang SY, Zhu H, Jin M, Su YH (2014a) Heterologous expression of an alligatorweed high-affinity potassium transporter gene enhances salinity tolerance in *Arabidopsis*. Am J Bot 101:840–850

Song ZZ, Yang Y, Xu JL, Ma RJ, Yu ML (2014b) Physiological and transcriptional response in the iron-sulphur cluster assembly pathway under abiotic stress in peach (*Prunus persica* L.) seedlings. Plant Cell Tissue Organ Cult 117:419–430

Song ZZ, Guo SL, Ma RJ, Zhang BB, Guo SL, Yu ML, Korir NK (2016a) Differential expression of iron–sulfur cluster biosynthesis genes during peach fruit development and ripening, and their response to iron compound spraying. Sci Hortic Amst 207:73–81

Song ZZ, Zhang BB, Zhang CH, Ma RJ, Yu ML (2016b) Differential expression of iron-sulfur cluster biosynthesis genes during peach flowering. Biol Plant 60(1):79–85

Song ZZ, Lin SZ, Fu JY, Chen YH, Zhang HX, Li JZ, Liang MX (2022) Heterologous expression of *ISU1* gene from *Fragaria vesca* enhances plant tolerance to Fe depletion in *Arabidopsis*. Plant Physiol Biochem 184:65–74

Song ZZ, Wang JP, Shi SP, Cao JW, Liu WH, Wu WH, Xiao HL, Tang ML (2023) Identification and cloning of Ferritin family genes in grape and response to compound amino acid-iron spraying during different fruit developmental stages. Sci Agric Sin 56(18):3629–3641 (**in Chinese**)

Tagliavini M, Rombolà AD (2001) Iron deficiency and chlorosis in orchard and vineyard ecosystems. Eur J Agron 15:71–92

Tagliavini M, Abadía J, Rombolà AD, Tsipouridis C, Marangoni B (2000) Agronomic means for the control of iron deficiency chlorosis in deciduous fruit trees. J Plant Nutr 23(11–12):2007–2022

Tang ML, Li YH, Chen YH, Han L, Zhang HX, Song ZZ (2020) Characterization and expression of ammonium transporter in peach (*Prunus persica*) and regulation analysis in response to external ammonium supply. Phyton Int J Exp Bot 89(4):925–941

Tiwari M, Sharma D, Dwivedi S, Singh M, Tripathi RD, Trivedi PK (2014) Expression in *Arabidopsis* and cellular localization reveal involvement of rice NRAMP, OsNRAMP1, in arsenic transport and tolerance. Plant Cell Environ 37:140–152

Vert G, Grotz N, Dédaldéchamp F, Gaymard F, Briat JF, Curie C (2002) IRT1, an *Arabidopsis* transporter essential for iron uptake from the soil and for plant growth. Plant Cell 14(6):1223–1233

Vert G, Barberon M, Zelazny E, Séguéla M, Briat JF, Curie C (2009) *Arabidopsis* IRT2 cooperates with the high-affinity iron uptake system to maintain iron homeostasis in root epidermal cells. Planta 229:1171–1179

Zelazny E, Vert G (2015) Regulation of iron uptake by IRT1: endocytosis pulls the trigger. Mol Plant 8:977–979

Zhang X, Zhang D, Sun W, Wang T (2019) The adaptive mechanism of plants to iron deficiency via iron uptake, transport, and homeostasis. Int J Mol Sci 20:2424

Zhang L, Zong YQ, Xu WH, Han L, Sun YZ, Chen ZH, Chen SL, Zhang K, Cheng JS, Tang ML, Zhang HX, Song ZZ (2021) Identification, cloning, and expression characteristics analysis of Fe-S cluster assembly genes in grape. Sci Agric Sin 54(23):5068–5082 (**in Chinese**)

Zhang Y, Shi XM, Lin SZ, Wang JP, Tang ML, Huang JF, Gao TP, Zhang HX, Song ZZ (2022) Heterologous expression of the *MiHAK14* homologue from *Mangifera indica* enhances plant tolerance to K^+ deficiency and salinity stress in *Arabidopsis*. Plant Growth Regul 98:39–49